

Uncertainty in pitch measurements of one-dimensional grating standards using a nanometrological atomic force microscope

Ichiko Misumi^{1,2}, Satoshi Gonda¹, Tomizo Kurosawa¹ and Kiyoshi Takamasu²

¹ National Metrology Institute of Japan, National Institute of Advanced Industrial Science and Technology (NMIJ/AIST), AIST Tsukuba Central 3, 1-1-1 Umezono, Tsukuba, Ibaraki 305-8563, Japan

² The University of Tokyo, 7-3-1 Hongo, Bunkyo, Tokyo 113-8656, Japan

E-mail: misumi.i@aist.go.jp

Received 3 October 2002, in final form 24 December 2002, accepted for publication 18 February 2003

Published 7 March 2003

Online at stacks.iop.org/MST/14/463

Abstract

Precision measurements of 240 nm-pitch one-dimensional grating standards were carried out using an atomic force microscope (AFM) with a high-resolution three-axis laser interferometer (nanometrological AFM). Laser sources of the three-axis laser interferometer in the nanometrological AFM were calibrated with an I₂-stabilized He–Ne laser at a wavelength of 633 nm. The results of the precision measurements using the nanometrological AFM have direct traceability to the length standard. The uncertainty in the pitch measurements was estimated in accordance with the *Guide to the Expression of Uncertainty in Measurement*. The primary source of uncertainty in the measurements was derived from interferometer nonlinearity, and its value was approximately 0.115 nm. Expanded uncertainty ($k = 2$) of less than 0.31 nm was obtained. It is suggested that the nanometrological AFM is a useful instrument for the nanometrological standard calibration.

Keywords: precision measurement, AFM, laser interferometer, calibration, standard, 1D grating, uncertainty, scales, nanometrology

(Some figures in this article are in colour only in the electronic version)

1. Introduction

The term ‘nanometrology’ has recently been used as one-dimensional metrology on the nanometrical scale. Standard samples for nanometrology, such as one-dimensional grating, two-dimensional grating, step height and line width are used to calibrate nanometrological instruments, for example, atomic force microscopes (AFMs), scanning electron microscopes (SEM) and diffractometers. Calibration of nanometrological standards is a key process for establishing the reliability of

these instruments and should be done using a high-precision length-standard-traceable instrument.

A number of national metrology institutes (NMIs) have developed nanometrological AFMs. A calibrated AFM (CAF) was developed at the National Institute of Standards and Technology (USA) in 1994 [1]. C-AFM has an XY-axis laser interferometer and a capacitance sensor in the Z-axis. The laser interferometer and capacitance sensor are calibrated using an I₂-stabilized He–Ne laser. A long-range AFM profiler was developed at the Swiss Federal Office of

Metrology and Accreditation (METAS, in Switzerland) in 1998 [2]. The scanning range of the X -axis leaf spring stage is long, approximately $380\ \mu\text{m}$, and the X position of the stage is detected and controlled using an X -axis laser interferometer. A metrology head is used as the Y - and Z -axes stage of the AFM profiler. A metrological scanning force microscope constructed at the Physikalisch-Technische Bundesanstalt (Germany) in 1998 [3] has an XYZ -axis laser interferometer and an XYZ -axis capacitance sensor for monitoring and control of the stage position, respectively. On the other hand, the Danish Institute of Fundamental Metrology (Denmark) developed methods for the accurate characterization of SPM by imaging and automated image processing using a commercial AFM with capacitive position sensors, in 1997 [4].

The National Metrology Institute of Japan, AIST (NMIJ/AIST), developed a 'nanometrological AFM' system with a ultra-high resolution three-axis laser interferometer in 1999 [5, 6]. The position of the scanning stage is monitored and servo-controlled using interferometer signals in real time. Since laser sources of the interferometer are calibrated with an I_2 -stabilized He-Ne laser, the uncertainties in measurement can be substantially minimized due to its direct traceability to the length standard compared to other metrological AFMs.

To establish metrological equivalence between the NMIs, various international key comparisons have been performed. Recently, supplementary key comparisons in the field of nanometrology have been carried out. Round-robin measurements of one-dimensional gratings with nominal pitches of 700 and 300 nm were completed, and the results are available from the database of the Bureau International des Poids et Mesures [7]. In the round-robin measurements, optical diffractometers and scanning probe microscopes (SPMs) were mainly used. NMIJ/AIST and the forenamed NMIs took part in the round-robin comparison using their metrological AFMs. The results of NMIJ/AIST are given under the former name of the institute, the National Research Laboratory of Metrology (NRLM). The measured values from NMIJ/AIST were close to the reference values of the round-robin measurements and the uncertainty in measurement obtained by NMIJ/AIST was the smallest in the results using SPMs, next to the pilot laboratory, METAS. As a result of a supplementary key comparison, metrological equivalence of the nanometrological AFM developed by NMIJ/AIST was certified.

It is becoming important to estimate the uncertainty in measurements as a criterion of the quality of a calibrated value. In order to ensure the validity of uncertainty estimation, it is necessary to make the estimation process transparent for each standard uncertainty component, for example, mathematical modelling, and the assumption of the distribution and calculation of the value of standard uncertainty. Several papers have shown dominating standard uncertainties of their pitch measurements with SPMs or resulting combined standard uncertainty [2, 8]. However, many scientists who deal with the calibration and levels of uncertainty of their own SPMs wish to find all possible sources of uncertainty and to evaluate them precisely. There are no reports which explain detailed processes of uncertainty evaluation in pitch measurements using SPMs. In this study, precision measurements of 240 nm-pitch one-dimensional grating standards were carried out using

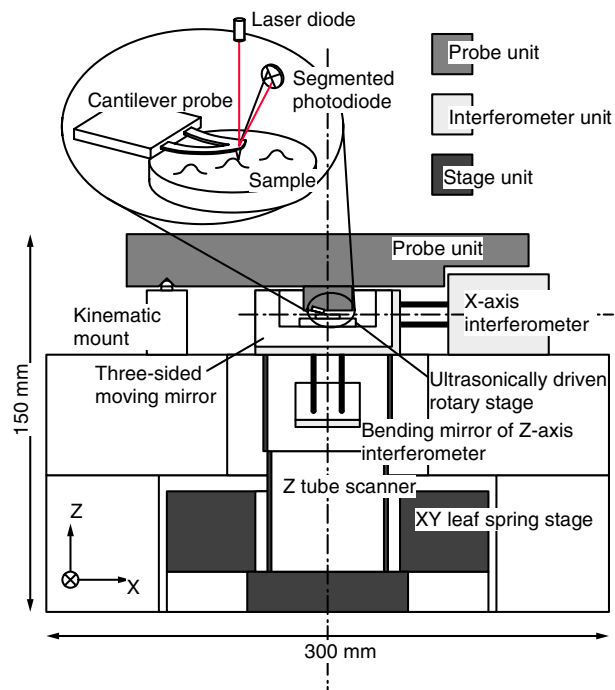


Figure 1. Cross-sectional drawing of the main unit of the nanometrological AFM. It consists of a stage unit, an AFM probe unit and interferometer units.

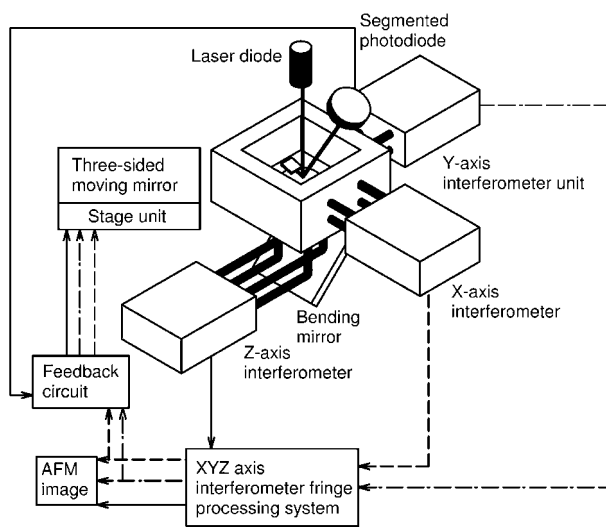


Figure 2. Block diagram of the nanometrological AFM system. The stage position is servo-controlled using the interferometer signals in real time.

the nanometrological AFM system, and any uncertainties in the pitch measurements were estimated in detail.

2. Experimental methods

2.1. Nanometrological atomic force microscope with a three-axis interferometer (nanometrological AFM)

A detailed description of the nanometrological AFM system is described elsewhere [5, 6]. Figures 1 and 2 show a cross-sectional drawing and a block diagram of the nanometrological AFM, respectively. The nanometrological AFM system is of

Table 1. Measurement conditions of one-dimensional grating standards using the nanometrological AFM.

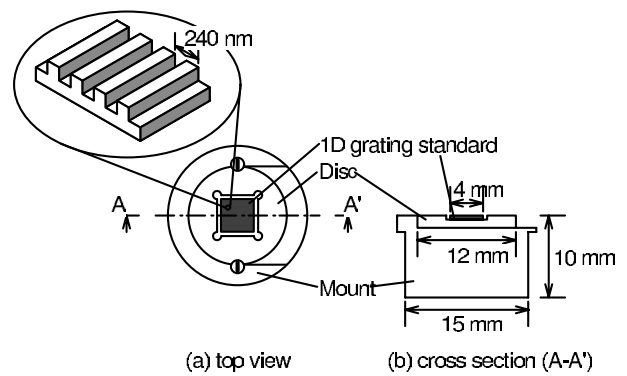
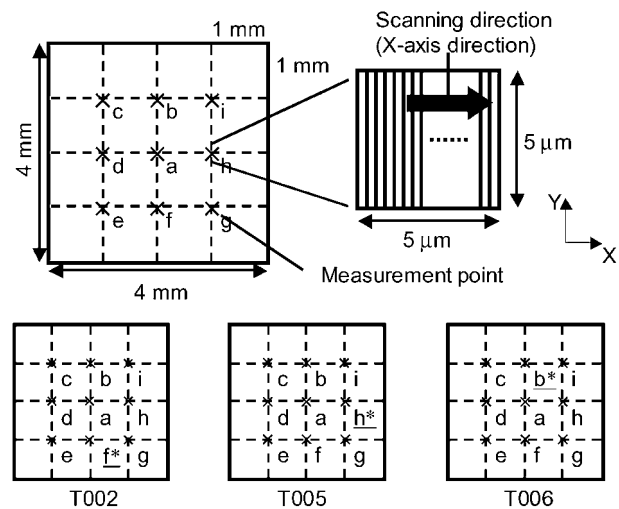
Number of samples	Measurement points	Measurement area (μm)	Number of scanning lines	Scanning speed ($\mu\text{m s}^{-1}$)
3	9	5×5	20	1
Sampling frequency of interferometer signals (kHz)	Spring constant of cantilever probe (N m^{-1})	Number of obtained pitches of one measurement point	Measurement time (min)	
1.125	0.01	≈ 440	≈ 5	

a stage scanning type and is operated in the contact AFM mode. The nanometrological AFM system consists of a stage unit, an AFM probe unit and an interferometer unit. The stage unit is comprised of a piezo-driven XY -axis leaf spring stage and a Z -axis scanner tube piezoactuator. The scanning area of this stage unit is approximately $17.5 \mu\text{m}$ (X) \times $17.5 \mu\text{m}$ (Y) \times $2.5 \mu\text{m}$ (Z). A bending mirror of the Z -axis interferometer is integrated into the Z -axis scanner tube. A three-sided moving mirror for the XYZ interferometer unit is set at the top of the Z -axis scanner. The interferometer has four optical paths in each axis and the total resolution of the interferometer unit is approximately 0.04 nm . A sample is set on an ultrasonically driven rotary stage, which is mounted inside the three-sided mirror and which adjusts the lateral rotational angle of the sample. Atomic force applied to a cantilever in the contact mode is detected using a conventional optical lever method. Laser sources of the interferometer unit are practical frequency-stabilized He-Ne lasers with a wavelength of 633 nm (model 117A, Spectra-Physics Ltd). The laser frequency is calibrated using an I_2 -stabilized He-Ne laser before measuring the one-dimensional grating pitch. The stage position is servo-controlled using the interferometer signals in real time, and the nanometrological AFM can meet the nanometrological standards for direct-length-standard-traceable calibration.

2.2. One-dimensional grating standards for a pitch of 240 nm

One-dimensional grating standards have been developed by Hitachi Ltd ('Standard Micro Scale', HJ-1000) [9] for the magnification calibration of the SEM and other nanometrological instruments. One-dimensional grating standards are fabricated by laser interferometer lithography and anisotropic chemical etching of (110) crystalline silicon. Grating patterns are fabricated over the entire surface. In these grating standards, a pitch of approximately 240 nm (approximately $4160 \text{ lines mm}^{-1}$) is obtained with an accuracy of within 1 nm (3σ) determined by the optical diffraction method. These gratings are made of conductive silicon crystal and are free from the build up charge under electron-beam irradiation. The depth of one-dimensional gratings is within 200 nm . High-contrast secondary electron signals can be obtained due to the high-aspect-ratio grating profile.

Figure 3 shows a schematic drawing of the one-dimensional grating standard with its mount with the top view shown in figure 3(a) and the cross section in figure 3(b). The one-dimensional grating standard is approximately 4 mm square. The one-dimensional grating standard is set at the top of an aluminium disc ($\phi = 12 \text{ mm}$) which is then


Figure 3. Schematic drawing of the one-dimensional grating standard with its mount: (a) top and (b) cross-sectional view.

Figure 4. Schematic drawing of measurement points. Grating patterns are fabricated over the entire surface. Nine measurement points are selected, as shown in the figure. Scanning area for each measurement point is $5 \mu\text{m}$ (X) \times $5 \mu\text{m}$ (Y). At the measurement points f^* in T002, h^* in T005 and b^* in T006, measurements were repeated three times.

placed in the sample holder of the nanometrological AFM for measurements.

2.3. Measurement procedure

Table 1 shows the measurement conditions of one-dimensional grating standards using the nanometrological AFM. Three samples were selected: T002, T005 and T006. Nine measurement points, as shown in the inset in figure 4, were selected. The measurement area at each measurement

Table 2. Order of measurements for three samples, T002, T005 and T006. The measurement points are shown in figure 4. The order was decided using a random number table. At measurement points f^* in T002, h^* in T005 and b^* in T006, the measurements were repeated three times (as shown in bold).

Order of measurements	Samples	Measurement points
1	T005	h^*
2	T005	h^*
3	T005	h^*
4	T005	f
5	T006	b^*
6	T006	b^*
7	T006	b^*
8	T002	h
9	T002	f^*
10	T002	f^*
11	T002	f^*
12	T006	h
13	T006	c
14	T002	g
15	T002	b
16	T002	a
17	T006	g
18	T002	e
19	T002	d
20	T002	c
21	T005	d
22	T005	a
23	T005	c
24	T006	e
25	T005	e
26	T006	i
27	T005	i
28	T005	b
29	T006	a
30	T002	i
31	T006	f
32	T006	d
33	T005	g

point was approximately $5 \mu\text{m}$ (X) \times $5 \mu\text{m}$ (Y) which was optimized in consideration of the trade-off between stable probe speed and desirable number of pitches in an image for statistic analyses. The larger measurement area yielded the larger number of pitches without any significant difference in average value. The stage was scanned at a speed of $1 \mu\text{m s}^{-1}$ and the scanning direction was perpendicular (X -axis direction) to the ribs of the grating patterns (Y -axis direction). One captured image had 32 profile lines. Twenty lines out of 32 were used for estimating the pitch values. The stage position was servo-controlled using position information obtained by the interferometer so that the scanning direction was kept in the X -axis direction. Yawing, rolling and pitching for X -axis direction scanning were estimated before measurement of the pitch values [5]. The sampling frequency of the XYZ interferometer signals was 1.125 kHz, which was decided according to the sampling interval of approximately 1 nm. In order to eliminate any damage to the sample surface, the spring constant of a cantilever probe must be quite small. For the measurements, a triangular microcantilever was selected and its nominal spring constant was 0.01 N m^{-1} (Veeco Ltd, formerly Thermomicroscopes Ltd MSCT-AUNM). The profiling data of 20 scanning lines were obtained in one measurement, and approximately 440 pitches

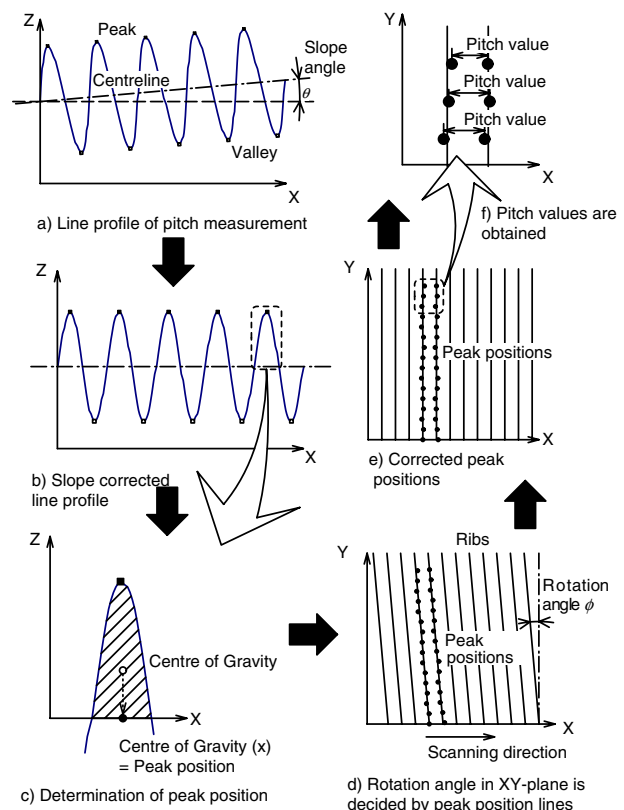


Figure 5. Calculation procedure for the pitch values.

were taken for 20 scanning lines. The average value of these pitches and the standard deviation were defined as the pitch value and the standard deviation at the measurement point. Measurements were performed in an air-controlled room at $20 \pm 0.5 \text{ }^\circ\text{C}$, $100 \pm 1 \text{ kPa}$ and $50 \pm 5\%$. Temperature, pressure and humidity in the measurement room were monitored during one measurement for approximately 5 min. The temperature in the neighbourhood of the sample was simultaneously measured.

To avoid any bias in the measurements, the order of measurements was decided using a random number table. Table 2 shows the order of measurements for three samples; T002, T005 and T006. The measurement points are shown in figure 4. At measurement points f^* in T002, h^* in T005 and b^* in T006, measurements were repeated three times to estimate the uncertainty in the repeatability of measurements at the same measurement point. Measurements were performed only once at the other measurement points.

3. Procedures of pitch value calculation and uncertainty estimation in measurement

3.1. Calculation procedures of pitch value

The calculation procedures of the pitch value shown in figure 5 were as follows.

3.1.1. Slope correction of the obtained line profile. Figure 5(a) shows 20 line profiles obtained by scanning. The centreline of the undulation of profiles is obtained by least

squares fitting using the peak and valley points. The slope of the line profiles is corrected by this centreline. Figure 5(b) shows the slope-corrected line profile. The ribs are not precisely parallel to the Y -axis direction. The correction of the rotational angle in the XY plane is required to make the ribs parallel to the Y -axis direction and to obtain the pitch values.

3.1.2. Peak position. Figure 5(c) shows an enlarged profile of figure 5(b). The area surrounded by the profile curve with the local peak point and the base line (X -axis) is calculated and the X position of the centre of gravity of this area is defined as the representative value of the peak position of each pitch.

3.1.3. Rotation angle of the sample in XY plane. Figure 5(d) shows the peak position line in the XY plane. The scanning direction (X -axis direction) and the ribs of the grating patterns (Y -axis direction) are not exactly perpendicular. When we plot the XY -coordinates of peak positions for 20 scanning lines of the same rib, the result is approximated as the straight line in figure 5(d). This eventually leads to a cosine error. The rotation angle is corrected using the slope of the approximated line as shown in figure 5(e).

3.1.4. Pitch value. The pitch value is taken to be the distance between two neighbouring peak positions. Approximately 440 pitch values are obtained and the average of these values is taken to be the pitch value at the measurement point.

3.2. Mathematical model of pitch calibration.

A single pitch value, Y_i , is derived from the interferometer signal count Z_i , length per counter L_u , correction coefficient of the refractive index of air C_i , a term for sample temperature correction C_t and a term for slope correction C_s . The mathematical model of pitch measurement is expressed as follows.

$$Y_i = Z_i L_u C_i C_t C_s. \quad (1)$$

Z_i can be obtained directly from the integrated values of up and down pulses of interferometer signals. The length per counter L_u , is derived by dividing the laser wavelength λ by an optical multiplication coefficient M_{opt} and an electrical multiplication coefficient M_{el} . M_{opt} is 4 since a laser beam travels four times along each axis in this interferometer unit (figure 2). M_{el} is 2048. L_u is expressed as

$$L_u = \lambda \left(\frac{1}{2M_{opt}} \frac{1}{M_{el}} \right). \quad (2)$$

C_i is given by Edlen's equation [10]. Slope correction and rotational angle correction are performed in the calculation procedure of pitch value. C_s is expressed as

$$C_s = \frac{1}{\cos \theta_i} \cos \varphi_i, \quad (3)$$

where θ_i is the slope angle and φ_i is the rotational angle in the XY plane. Measurements are made in the air-controlled room at approximately 20 °C. Thermal expansion of the sample,

Table 3. Sources of uncertainty and standard uncertainty components in pitch measurements using the nanometrological AFM.

Sources of uncertainty	Standard uncertainty component
(1) Pitch measurement	
(i) Repeatability	s_i
(ii) Nonuniformity	s_p
(2) Laser interferometer	
(i) Frequency variation of laser	f_i
(ii) Frequency stability of laser	f_{li}
(iii) Changes in the dead path (temperature)	δd_T
(iv) Changes in the dead path (thermal expansion)	δd_α
(v) Interferometer resolution	δl_{RE}
(vi) Cosine error in optical alignment	δl_{CO}
(vii) Abbe error	δl_{Ai}
(viii) Change in optical path	δl_{OP}
(ix) Interferometer nonlinearity (cyclic error)	δl_{NL}
(3) Refractive index of air	
(i) Refractive index of air (temperature)	n_t
(ii) Refractive index of air (humidity)	n_h
(iii) Refractive index of air (pressure)	n_p
(4) Sample temperature	
(i) Difference in the sample temperature	$20 - t_g$
(ii) Thermal expansion	α
(5) Slope correction	
(i) Cosine error (vertical inclination)	δl_{CVi}
(ii) Cosine error (lateral inclination)	δl_{CLi}

derived from a few temperature differences, is corrected as follows:

$$C_t = 1 + \alpha s_i (T_i - 20). \quad (4)$$

The mathematical model of pitch measurement is expressed using equations (1)–(4).

$$Y_i = Z_i \lambda \left(\frac{1}{2M_{opt}} \frac{1}{M_{el}} C_i \right) \frac{1}{\cos \theta_i} \cos \varphi_i [1 + \alpha s_i (T_i - 20)]. \quad (5)$$

3.3. Estimation of uncertainty in measurement

The uncertainty in one-dimensional grating pitch measurement using the nanometrological AFM system is estimated. The sources of uncertainty are given based on the mathematical model given in equation (5). The sources of uncertainty are divided into five classes as follows.

- Pitch measurement (Z_i)
- Laser interferometer (λ)
- Refractive index of air (C_i)
- Sample temperature (C_t)
- Slope correction (C_s).

The estimation method of uncertainty in measurement and its expression are based on the Guide to the Expression of Uncertainty in Measurement (GUM) [11]. The sources of uncertainty and standard uncertainty components in pitch measurements are shown in table 3.

3.3.1. Pitch measurement. Two sources of uncertainty of pitch measurement are obtained.

- (i) s_r , is derived from the repeatability of pitch measurement. At point f^* in T002, h^* in T005 and b^* in T006, three pitch measurements were made. The standard uncertainty derived from the repeatability of measurements is decided from the dispersion of the three pitch values at the same measurement point.
- (ii) s_p , is derived from the nonuniformity of the sample. The nonuniformity is given by the standard deviation of the nine pitch values obtained at point a to point i.

3.3.2. *Laser interferometer.* Nine sources of uncertainty of the laser interferometer are estimated as follows.

- (i) Uncertainty derived from frequency variation of laser f_i is determined from the maximum Allan variance at various gate times.
- (ii) Uncertainty derived from the frequency stability of laser f_{li} is estimated from the maximum change in the measured frequency over two years.
- (iii) Uncertainty derived from the changes in the dead path (temperature change component) δd_T is determined from the maximum temperature changes in the interferometer base plate.
- (iv) Uncertainty derived from the changes in the dead path (thermal expansion of interferometer base plate component), δd_α , is evaluated from the unreliability of the thermal expansion coefficient of the base plate.
- (v) Uncertainty derived from interferometer resolution δl_{RE} is defined as one up and down pulse of the interferometer signal.
- (vi) Uncertainty derived from the cosine error in optical alignment δl_{CO} is given by the maximum measured value during the alignment of the optic parts.
- (vii) Uncertainty derived from the Abbe error δl_{Ai} is estimated using equation (6) from figure 6 as follows:

$$\delta l_{Ai} = \frac{d \tan \phi + D \left(\frac{1}{\cos \phi} - 1 \right)}{\sqrt{3}} \quad (6)$$

where d is the Abbe offset which is estimated from the maximum value of 0.5 mm, D is the distance between the measurement point and the moving mirror surface, which is 23 mm. ϕ is the rotation angle of the stage, which is 3.23×10^{-5} arcsec nm^{-1} . The distribution is assumed to be rectangular and it is divided by the square root of 3 in order to obtain the uncertainty value.

- (viii) Uncertainty derived from changes in the optical path δl_{OP} is determined from the stage rotation during stage scanning. The alignment error angle is used as the offset. δl_{OP} is obtained using equation (7) from figure 7:

$$\delta l_{OP} = \frac{4L \left(\frac{1}{\cos(\theta+2\phi_p)} - \frac{1}{\cos \theta} \right)}{\sqrt{3}}, \quad (7)$$

where L is the distance between a moving mirror surface and a beam splitter that divides the laser beam into the reference mirror direction and the moving mirror direction in the X -axis interferometer, which is 24 mm. θ is an alignment error angle and its value is 2.83×10^{-2} arcdeg. ϕ_p is the rotational angle while the stage scans a single pitch distance.

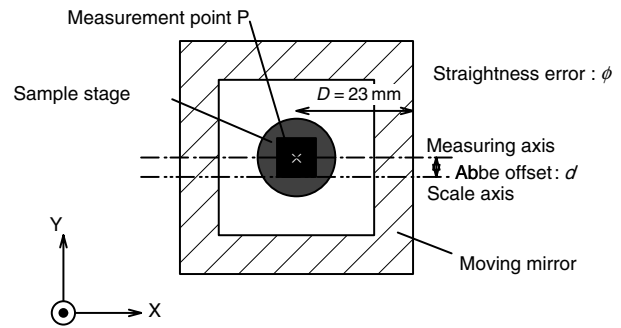


Figure 6. The Abbe error.

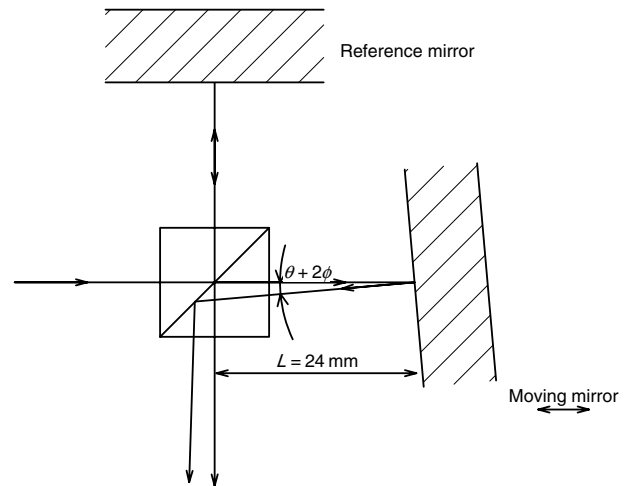


Figure 7. The uncertainty derived from changes in the optical path.

- (ix) Uncertainty derived from interferometer nonlinearity (cyclic error) δl_{NL} is given by the following procedure. The stage is driven in the X -axis direction by triangular wave signals and its displacement is detected by the X -axis interferometer. The least-squares-fit curve of the obtained interferometer signals is calculated and the obtained residual error is used as the interferometer nonlinearity.

3.3.3. *Refractive index of air.* Three sources of uncertainty are derived from the change in the refractive index of air. Data for temperature, humidity and air pressure in the experimental room are approximated to have a rectangular distribution using temperature, humidity and air pressure data, respectively gathered during pitch or other measurements throughout one year. The change in the refractive index of air is calculated using Edlen's equation with the humidity and pressure of air being fixed at the middle value of distribution and only the temperature of air being changed. The source of uncertainty derived from the change in the refractive index of air (temperature component) is decided using the change in temperature. The other two sources of uncertainty derived from the change in the refractive index of air (humidity component and pressure component) are estimated in the same manner.

3.3.4. *Sample temperature.* Two sources of uncertainty derived from the sample temperature are estimated.

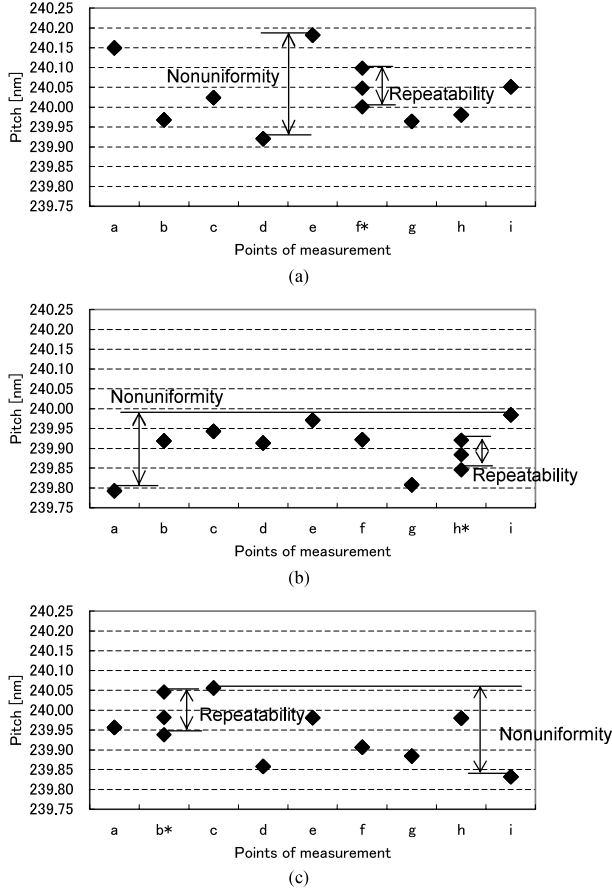


Figure 8. The pitch values at all measurement points in samples T002 (a), T005 (b) and T006 (c).

- (i) $20 - t_g$ is derived from the change in sample temperature in one year.
- (ii) α is given by the thermal expansion of the sample. The coefficient of thermal expansion of silicon was $2.6 \times 10^{-6} \text{ K}^{-1}$ as measured by NMIJ/AIST [12].

3.3.5. Slope correction. Two sources of uncertainty derived from slope corrections are estimated.

- (i) δl_{CVi} is derived from the cosine error of vertical inclination and is determined from the centreline slope of 1 line profile. This slope angle is represented in equation (3) as θ_i . The maximum slope coefficient is decided as the standard uncertainty component δl_{CVi} .
- (ii) δl_{CLi} is derived from the cosine error of lateral inclination and is determined from the rotational angle ϕ_i in equation (3). The average correction coefficient of the rotational angle is taken to be the standard uncertainty component δl_{CLi} .

4. Results

Figures 8(a)–(c) show the results for the measured pitch values of samples T002, T005 and T006, respectively. Nonuniformity, i.e., dispersion of measured pitch values in a sample, was approximately two times greater than

repeatability, the dispersion of measured pitch values at one measurement point of a sample. The dispersion behaviours of measured pitch values are different between samples T002, T005 and T006, and there is no measurement-point dependence of the dispersion. This is probably due to the uniformity of dispersion in the measured pitch values. On the other hand, dispersion in the repeatability of three measurements in the same measurement point seems to be derived from the probing error.

Table 4 shows the estimated results of uncertainty in the measurements for sample T002. The combined uncertainty u_c is the square root of the sum of squares of each standard uncertainty u_i and it is expressed, for sample T002, as

$$u_c = \sqrt{\sum u_i^2} = \sqrt{(1.55 \times 10^{-1})^2 + (9.89 \times 10^{-6} \times p)^2} \quad (8)$$

where p is the pitch value (in nm).

The major source of uncertainty was derived from the interferometer nonlinearity, δl_{NL} and the value of standard uncertainty was approximately 0.115 nm. This source of uncertainty was estimated from the residuals after subtracting the polynomial fitting of the curve from the displacement curve. The second major uncertainty was derived from the nonuniformity of a sample s_p and its value was about 8.71×10^{-2} nm. The third major uncertainty was derived from measurement repeatability s_i and its value was approximately 4.88×10^{-3} nm. The second and third major uncertainties are shown in figure 8. The interferometer resolution δl_{RE} designed during the development of this system, was the fourth major source of uncertainty. The fifth major uncertainty was a result of the frequency variation of the laser f_i . The major sources of uncertainty in measurements seem to be due to the interferometer nonlinearity and frequency variation of the laser, which are derived from laser interferometers used on the sub-nanometrical scale.

Table 5 shows the pitch values p (nm), effective degrees of freedom v_{eff} , combined standard uncertainty $u_c(p)$ (nm) and expanded uncertainty $U(p)$ (nm), respectively. The expanded uncertainty of sample T002 was approximately 0.310 nm and which was less than 0.2% of the pitch value, p . The measurement and uncertainty results obtained meet the requirements for nanometrical order precision measurements and nanometrological calibration.

5. Discussion

We attempted to calibrate one-dimensional gratings using nanometrological AFM. We measured the pitch values of one-dimensional gratings with an expanded uncertainty of approximately 0.310 nm for sample T002. The value of the expanded uncertainty is less than 0.2% of the pitch value p and satisfies the requirement for the precision nanometrical measurements. The major source of uncertainty derived from the laser interferometer nonlinearity and the value of the standard uncertainty was approximately 0.115 nm. This value was larger than other sources of uncertainty, the nonuniformity of the sample and measurement repeatability. Precise estimation of uncertainty in measurements is useful because we can then identify the points that must be improved in the instrument.

Table 4. Budget table of uncertainty in measurements of sample T002.

Source of uncertainty	Standard uncertainty component, u	Value of standard uncertainty, u	Type	Distribution	Degrees of freedom v_i	Sensitivity coefficient c_i	Components of combined standard uncertainty $u_i = c_i u$ (nm)
(1) Pitch measurement							
(i) Repeatability	s_i	4.88×10^{-2} nm	A		2	1	4.88×10^{-2} (3rd)
(ii) Nonuniformity	s_p	8.71×10^{-2} nm	A		8	1	8.71×10^{-2} (2nd)
(2) Laser interferometer							
(i) Frequency variation of laser	f_i	1.24×10^{-1} MHz	B	R	200	9.75×10^{-2}	1.21×10^{-2} (5th)
(ii) Frequency stability of laser	λ_i	5.00×10^{-5} nm	B	R	200	$9.12 \times 10^{-4} \times p$	1.09×10^{-5}
(iii) Changes in the dead path (temperature)	δd_T	3.20 K	B	R	12.5	3.65×10^{-7}	1.17×10^{-6}
(iv) Changes in the dead path (thermal expansion)	δd_α	3.02×10^{-5} K ⁻¹	B	R	200	3.87×10^{-2}	1.17×10^{-6}
(v) Interferometer resolution	δl_{RE}	3.86×10^{-2} nm	B	R	200	5.77×10^{-1}	2.23×10^{-2} (4th)
(vi) Cosine error in optical alignment	δl_{CO}	2.83×10^{-2} arcdeg	B	R	200	$7.06 \times 10^{-8} \times p$	1.69×10^{-5}
(vii) Abbe error	δl_{Ai}	3.23×10^{-5} arcsec nm ⁻¹	B	R	200	336	1.09×10^{-2}
(viii) Changes in the optical path	δl_{OP}	3.23×10^{-5} arcsec nm ⁻¹	B	R	200	63.8	2.06×10^{-3}
(ix) Interferometer nonlinearity	δl_{NL}	0.20 nm	B	R	200	5.77×10^{-1}	1.15×10^{-1} (1st)
(3) Refractive index of air							
(i) Refractive index of air (temperature)	n_t	1.20 K	B	R	12.5	$5.47 \times 10^{-7} \times p$	1.58×10^{-4}
(ii) Refractive index of air (humidity)	n_a	3.50%	B	R	12.5	$6.17 \times 10^{-9} \times p$	5.18×10^{-6}
(iii) Refractive index of air (pressure)	n_p	1.50 kPa	B	R	12.5	$1.54 \times 10^{-6} \times p$	5.54×10^{-4}
(4) Sample temperature							
(i) Difference in the sample temperature	$20 - t_g$	3.20 K	B	R	12.5	$150 \times 10^{-6} \times p$	1.15×10^{-3}
(ii) Thermal expansion	α	2.60×10^{-6} K ⁻¹	B	R	200	$1.85 \times p$	1.15×10^{-3}
(5) Slope correction							
(i) Cosine error (vertical inclination)	δl_{CVi}	4.83×10^{-6}	A		19	$4.83 \times 10^{-6} \times p$	1.16×10^{-3}
(ii) Cosine error (lateral inclination)	δl_{CLi}	4.75×10^{-6}	A		19	$4.75 \times 10^{-6} \times p$	1.14×10^{-3}

Combined standard uncertainty, u_c , given as per equation (8), i.e.

$$u_c = \sqrt{\sum u_i^2} = \sqrt{(1.55 \times 10^{-1})^2 + (9.89 \times 10^{-6} \times p)^2} \text{ (nm)}$$

(p in nm).

Table 5. Measurement results and uncertainties for each sample.

Sample	Pitch value, p (nm)	Combined standard uncertainty, u_c (nm)	Effective degrees of freedom, v_{eff}	Expanded uncertainty ($k = 2$), U (nm)
T002	240.03	0.155	53.0	0.310
T005	239.90	0.141	90.4	0.283
T006	239.94	0.151	54.9	0.301

There are a number of problems in reducing the uncertainty. Polarization elements such as the beam splitter, wave plate and cube corner reflectors lead to periodic error [13] of the laser interferometer. Accordingly, it is necessary to use high-quality optical elements. The optical arrangement demands that the measurement and reference beams do not cross each other along the optical path. If the interferometer is symmetric, uncertainty derived from the thermal expansion of

the XY stage is compensated. Uncertainty induced in a long dead path of the interferometer can be reduced using high-stability lasers offset-locked on the I₂-stabilized He–Ne laser. The contact mode should be changed to the tapping mode to avoid any damage to the sample.

It is important to carry out precise measurements conforming to various nanometrology standards using length-standard-traceable instruments according to the users' requirements. The precise estimation of measurement uncertainty outlined in this study is useful for the following two reasons: we can identify future problems that need to be solved, and users of nanometrological standards can identify the method of calibration based on their 'budget' of uncertainty.

6. Conclusions

Precision measurements of 240 nm-pitch one-dimensional grating standards were carried out using an AFM system with

a high-resolution three-axis laser interferometer (nanometrological AFM). The average value of the pitch and the expanded uncertainty in the measurements were 239.96 nm and less than 0.310 nm, respectively. The major sources of uncertainty in the measurements were derived from the interferometer nonlinearity and nonuniformity of the sample. The results satisfy the requirement for precision measurement to nanometrical order and calibration to nanometrological standards.

Acknowledgment

The authors would like to thank Hitachi Co. Ltd for supplying the samples ('Standard Micro Scale' HJ-1000).

References

- [1] Schneir J, McWaid T H, Alexander J and Wilfley B P 1994 Design of an atomic force microscope with interferometric position control *J. Vac. Sci. Technol. B* **12** 3561
- [2] Meli F and Thalmann R 1998 Long-range AFM profiler used for accurate pitch measurements *Meas. Sci. Technol.* **9** 1087
- [3] Bienias M, Gao S, Hasche K, Seemann R and Thiele K 1998 A metrological scanning force microscope used for coating thickness and other topographical measurements *Appl. Phys. A* **66** S837
- [4] Jorgensen J F, Jensen C P and Garnaes J 1998 Lateral metrology using scanning probe microscopes, 2D pitch standards and image processing *Appl. Phys. A* **66** S847
- [5] Gonda S, Doi T, Kurosawa T, Tanimura Y, Hisata N, Yamagishi T, Fujimoto H and Yukawa H 1999 Real-time, interferometrically measuring atomic force microscope for direct calibration of standards *Rev. Sci. Instrum.* **70** 3362
- [6] Gonda S, Doi T, Kurosawa T, Tanimura Y, Hisata N, Yamagishi T, Fujimoto H and Yukawa H 1999 Accurate topographic images using a measuring atomic force microscope *Appl. Surf. Sci.* **144/145** 505
- [7] <http://www.bipm.org/>
- [8] Chernof D A, Lohr J D, Hansen D P and Lines M 1997 High-precision calibration of a scanning probe microscope (SPM) for pitch and overlay measurements *Proc. SPIE* **3050** 243-9
- [9] Nakayama Y and Toyoda K 1994 New submicron dimension reference for electron-beam metrology system *Proc. SPIE* **2196** 74
- [10] Edlen B 1966 The refractive index of air *Metrologia* **2** 71
- [11] ISO 1993 BIPM, IEC, IFCC, ISO, IUPAC, IUPAP, OIML *Guide to the Expression of Uncertainty in Measurement*
- [12] Okaji M and Imai H 1992 High precision dilatometer by means of optical heterodyne interferometer *Netsu Bussei* **6** 83 (in Japanese)
- [13] Bobroff N 1993 Recent advances in displacement measuring interferometry *Meas. Sci. Technol.* **4** 907